www.jmolecularsci.com

ISSN:1000-9035

# Experimental and Theoretical study on 2-(5-bromo-2-(trifluoromethoxy)phenyl)-5-(thiophen-2-yl)-1,3,4-oxadiazole

Savariyappan Albert Nikson<sup>1</sup>, Richard Rajkumar Siluvairaj<sup>1</sup>, David Amalraj Savarimuthu<sup>1</sup>, T. Antony Sandosh<sup>1</sup>, Chinnappan Adaikalaraj<sup>1</sup>, S. Manivarman <sup>2\*</sup>,

<sup>1</sup>PG and Research Department of Chemistry, St. Joseph's College of Arts and Science (Autonomous), Cuddalore, Tamil Nadu, 607001, India.

<sup>2</sup>PG and Research Department of Chemistry, Government Arts College, C-Mutlur, Chidambaram, Tamil Nadu, 608102, India...

Email: drsmgac@gmail.com

#### Article Information

Received: 15-06-2025 Revised: 28-06-2025 Accepted: 16-07-2025 Published: 04-08-2025

#### **Keywords**

DFT; NBO analysis; HOMO– LUMO; FMO; NLO properties; Hyperpolarizability; Molecular electrostatic potential (MEP); Fukui function; Aromaticity; HOMA index; Global reactivity descriptors; Quantum chemical analysis.

#### **ABSTRACT**

A detailed quantum chemical investigation was carried out on the title molecule using density functional theory (DFT) at the B3LYP/6-311G(d,p) level. Natural Bond Orbital (NBO) analysis revealed significant donor-acceptor intramolecular charge transfer (ICT) through interactions, with notable second-order perturbation energies indicating strong stabilization via hyperconjugation and delocalization. Frontier Molecular Orbital (FMO) calculations determined a HOMO-LUMO energy gap of 3.2511 eV, suggesting favorable charge transfer characteristics and good chemical stability. Global reactivity parameters, including ionization potential, electron affinity, electronegativity, and electrophilicity index, were evaluated to understand the compound's reactivity and electronic features. Nonlinear optical (NLO) property calculations showed that the first-order hyperpolarizability is comparable to that of urea, highlighting its potential as a candidate for optoelectronic applications. Furthermore, HOMA values confirmed the aromatic nature of specific moieties, while Fukui function analysis and Molecular Electrostatic Potential (MEP) mapping provided insights into nucleophilic and electrophilic reactive sites. These findings demonstrate the multifunctional nature of the molecule, with potential utility in both material science and pharmaceutical domains.

## ©2025 The authors

This is an Open Access article distributed under the terms of the Creative Commons Attribution (CC BY NC), which permits unrestricted use, distribution, and reproduction in any medium, as long as the original authors and source are cited. No permission is required from the authors or the publishers.(https://creativecommons.org/licenses/by-nc/4.0/)

#### 1. INTRODUCTION

Oxadiazole has a key function in ligand binding and pharmacophores<sup>1</sup>. It is an aromatic heterocyclic linking group that may join a range of substituents and has the same biological activity as carbamates, amides, and esters <sup>2</sup>. 1,3,4-oxadiazole and its derivatives have been shown to have antibacterial, anti-inflammatory. anti-tubercular. anti-HIV. antifungal, cathepsin K (Cat K) inhibitory, monoamine oxidase inhibitory, anti-diabetic, tyrosinase inhibitory, antioxidant, and anticancer properties<sup>3–5</sup>. Additionally, some of the currently used pharmacological compounds include 1,3,4oxadiazole rings, such as the antiviral medicine Raltegravir<sup>6</sup>, the anticancer drug Zibotentan <sup>7</sup>, the antihypertensive agent Nesapidil<sup>8</sup>, and the hypnotic drug Fenadiazole<sup>9</sup> (Fig. 1).

Figure 1. Biologically active 1,3,4-oxadiazole derivatives

Similarly, because to its many useful applications in solar cells, thin-film field-effect transistors, and organic electronics, thiophene-based derivatives have become more important in materials science and technology. Particularly, the characteristics of compounds based on thiophene are employed to track biological processes involving macromolecules like DNA and proteins <sup>10</sup>. The pharmacokinetic and pharmacodynamic characteristics of a medication are improved by thiophene, which has been shown to be a potential isosteric 11. Additionally, adding fluorine to biologically active medications improves their pharmacological characteristics, and at least one fluorine atom is present in 15% of all drugs [12]. The factors previously mentioned prompted us to develop a compound named 2-(5-bromo-2-(trifluoromethoxy)phenyl)-5-(thiophen-2-yl)-1,3,4oxadiazole (BPTO), which incorporates a fluorine atom alongside the thiophene and 1,3,4-oxadiazole ring structures.

Organic nonlinear optical (NLO) materials have garnered a lot of attention in the past two decades because of their optical, electrical, electrochemical characteristics. The development of organic materials with significant nonlinear optical coefficients through improved design and synthesis has drawn a lot of interest recently 13. In organic materials, the prolonged delocalized aromatic conjugation is a structural need for the observation of substantial third-order NLO effects. Furthermore, current experimental methods and theoretical tools indicate that  $\pi$ -conjugated heteroatomic systems with intramolecular charge transfer capabilities are viable options for modern organic electronics and photonics <sup>14–17</sup>.

To improve electrical characteristics, oxadiazole derivatives are essential. Using 1,3,4-oxadiazole derivatives, for examples, Deshapande *et al.* <sup>18</sup> used 1, 3,4-oxadiazole derivatives to synthesize

fluorescent optoelectronic compounds with applications. Liu et al. used 1,3,4-oxadiazole derivatives to trap Cu<sup>2+</sup> ions <sup>19</sup>. Westphal *et al.*<sup>20</sup> investigated the utilization of liquid crystals derived from 1,3,4-oxadiazole in NLO. Paun et al. employed small compounds and polymers based on 1,3,4-oxadiazole for their OLEDs <sup>21</sup>. To the experimental substantiate findings. DFT/B3LYP/6-311 G(d,p) was employed to investigate the synthesis of a new compound. 22-23

#### 2. Experimental:

All the chemicals (solvents and reagents) were purchased from Hi-media and Sigma/Aldrich. The synthesized compounds were scaled for yield, purified and identified by TLC. The infrared spectra (KBr) were recorded using Shimadzu 8201PC instrument operating on 4000-400 cm-1. The proton NMR and Carbon NMR were recorded using Agilent V NMRS-400 instrument with CDCl<sub>3</sub> and the chemical shifts are expressed in ppm.

# 2.1. Synthesis of 2-(5-bromo-2-(trifluoromethoxy)phenyl)-5-(thiophen-2-yl)-1,3,4-oxadiazole (3):

In a round bottom flask, as shown in **Scheme-1** aryl acid hydrazide (1 mmol) was dissolved in phosphorous oxychloride (5mL) and 5-bromo-2-(2,2,2-trifluoromethoxy)benzoic acid (1 mmol) was added. This mixture was refluxed at mild condition. After completion of the reaction, the mixture was cooled to room temperature and poured into crushed ice. The content was neutralized with sodium bicarbonate solution (20%), a solid mass separated out. This was filtered, washed and recrystallized by using ethanol to give 2-(5-bromo-2-(trifluoromethoxy)phenyl)-5-(thiophen-2-yl)-1,3,4-oxadiazole. The assigned structure and

1,3,4-oxadiazole. The assigned structure and molecular formula of the newly synthesized compounds BPTO were confirmed by melting point, elemental analyses, FT-IR, 1H NMR and 13C NMR data.

Scheme 1. Synthesis scheme for 2-(5-bromo-2-(trifluoromethoxy)phenyl)-5-(thiophen-2-yl)-1,3,4-oxadiazole

2.2 Speactral data of 2-(5-bromo-2-(trifluoromethoxy)phenyl)-5-(thiophen-2-yl)-**1,3,4-oxadiazole**: IR (KBr):  $v \sim (cm^{-1})$  1637, 1583, 1471, 1239, 1149; <sup>1</sup>H NMR (400 MHz, CDCl<sub>3</sub>) δ: 8.29 (d, J=8.0 Hz, 1H), 7.97 (d, J=8.4 Hz, 1H), 7.68 (s, 1H), 7.20-6.14 (m, 2H), 6.99 (d, *J*=8.0 Hz, 1H); <sup>13</sup>C NMR (100 MHz, CDCl<sub>3</sub>) δ: 161.76, 160.96, 158.04, 135.88, 133.20, 124.37, 121.60, 116.23, 115.61, 114.41.

#### 2.3 **Computational details:**

The quantum chemical calculations of BDMB were performed with the DFT/B3LYP/6- 311G (d,p) level of theory by using the Gaussian 09 program <sup>24</sup>. <sup>25-26</sup>. The optimized structural package parameters were used in the vibrational wavenumber calculations to characterize all stationary points as minima. Harmonic vibrational wavenumber calculations and their associated FT-IR intensities and Raman depolarization ratios were carried out. The vibrational modes were assigned based on potential energy distribution by using VEDA4 program <sup>27</sup>.

### 3. RESULTS AND DISCUSSION 3.1 DFT analysis of BPTO

#### **Optimized parameters** 3.1.1

The computed optimized geometrical parameters of 2-(5-bromo-2-(trifluoromethoxy)phenyl)-5-

(thiophen-2-yl)-1,3,4-oxadiazole are summarized in Table 1. The optimized molecular structure is illustrated in Figure 1, and the corresponding

minimum energy conformation is confirmed by the potential energy surface scan shown in Figure 2. The molecule comprises a phenyl ring, a thiophene ring, and a 1,3,4-oxadiazole ring. It contains two C-S-C linkages, two C=N bonds, one C-Br bond, three C-F bonds, six C-H bonds, and eleven C-C bonds. The C-C bond lengths within the phenyl ring range from 1.386 to 1.4098 Å. Notably, the C14-C15 and C14-C16 bonds are elongated (1.4014 Å and 1.4098 Å, respectively), likely due to the electron-withdrawing effects of substituents in the ortho position. The computed C=N bond lengths are approximately 1.31 Å, which is slightly shorter than experimental X-ray diffraction (XRD) values reported in the literature  $(1.373-1.364 \text{ Å})^{28}$ . The C–O bond distances within the oxadiazole ring range from 1.3981 to 1.4248 Å, closely matching the reported value of 1.37 Å [28]. The N5-N4 bond length is found to be 1.4235 Å, slightly longer than the literature value of 1.4221 Å <sup>28</sup>. Furthermore, a significant dihedral angle of 82.66° is observed between the trifluoromethoxy group and the phenyl ring, indicating a noticeable twist in the molecular conformation due to steric and electronic effects <sup>29</sup>. The molecule exhibits shortening of bond and elongation of bond as an evident for presence of Blue shift (negative) and Red shift (positive) hydrogen bonding. The potential Blue shift hydrogen bonded atom pairs C17-H21--→F26, where the bond length C17-H21 is found to be decreased 1.0691 A°.

Bond	Bond length (A)	Bond	Bond angle (0)	Bond	Dihedral angle (°)
C1-O2	1.38	O2-C1-N4	111.66	N4-C1-O2-C3	-0.18
C1-N4	1.28	O2-C1-C6	117.44	C6-C1-O2-C3	179.72
C1-C6	1.43	N4-C1-C6	130.90	O2-C1-N4-N5	0.07
O2-C3	1.38	C1-O2-C3	103.91	C6-C1-N4-N5	-179.81
C3-N5	1.27	O2-C3-N5	111.59	O2-C1-C6-C7	0.04
C3-C14	1.45	O2-C3-C14	121.08	O2-C1-C6-S8	-179.91
N4-N5	1.45	N5-C3-C14	127.31	N4-C1-C6-C7	179.92
C6-C7	1.34	C1-N4-N5	106.17	N4-C1-C6-S8	-0.03
C6-S8	1.79	C3-N5-N4	106.67	C1-O2-C3-N5	0.22
C7-C9	1.44	C1-C6-C7	126.12	C1-O2-C3-C14	178.72
C7-H10	1.07	C1-C6-S8	121.48	O2-C3-N5-N4	-0.18
S8-C11	1.79	C7-C6-S8	112.39	C14-C3-N5-N4	-178.57
C9-C11	1.34	C6-C7-C9	113.17	O2-C3-C14-C15	9.90
C9-H12	1.07	C6-S8-C11	88.59	O2-C3-C14-C16	-170.15

C11-H13	1.07	C7-C9-C11	113.55	N5-C3-C14-C15	-171.86
C14-C15	1.38	C3-C14-C15	123.42	N5-C3-C14-C16	8.10
C14-C16	1.39	C3-C14-C16	117.95	C1-N4-N5-C3	0.07
C15-C17	1.38	C15-C14-C16	118.62	C1-C6-C7-C9	-179.95
C15-O23	1.40	C14-C15-C17	121.06	S8-C6-C7-C9	0.00
C16-C18	1.37	C14-C15-O23	120.36	C1-C6-S8-C11	179.95
C16-H19	1.07	C17-C15-O23	118.52	C7-C6-S8-C11	-0.01
C17-C20	1.38	C14-C16-C18	120.44	C6-C7-C9-C11	0.01
C17-H21	1.07	C15-C17-C20	119.75	C3-C14-C15-C17	-179.18
C18-C20	1.38	C16-C18-C20	120.37	C3-C14-C15-O23	3.82
C18-Br24	1.92	C16-C18-Br24	119.82	C16-C14-C15-C17	0.86
C20-H22	1.07	C20-C18-Br24	119.80	C15-C14-C16-C18	-0.69
O23-C25	1.35	C17-C20-C18	119.75	C14-C15-C17-C20	-0.40
C25-F26	1.33	C15-O23-C25	122.04	O23-C15-C17-C20	176.66
C25-F27	1.34	O23-C25-F26	108.92	C14-C15-O23-C25	-99.07
C25-F28	1.34	O23-C25-F27	111.07	C17-C15-O23-C25	83.85
		O23-C25-F28	112.40	C14-C16-C18-C20	0.06
		F26-C25-F27	108.10	C14-C16-C18-Br24	-179.85
		F26-C25-F28	108.97	C16-C18-C20-C17	0.42
		F27-C25-F28	107.27	Br24-C18-C20-C17	-179.67
				C15-O23-C25-F26	159.56
				C15-O23-C25-F27	-81.49
				C15-O23-C25-F28	38.69

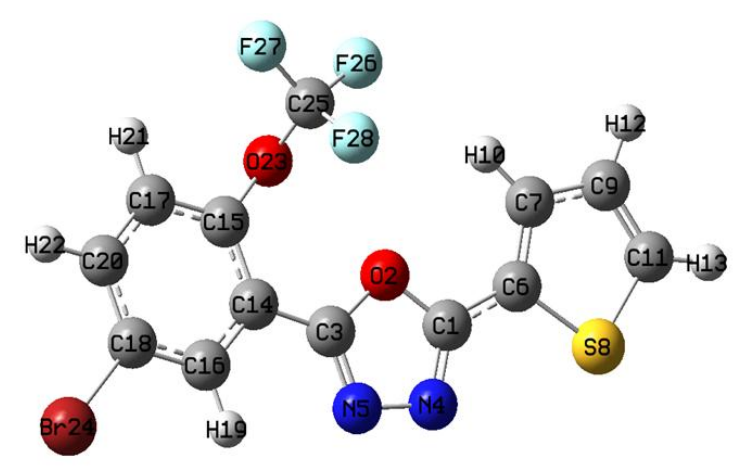


Figure 2: Optimized geometry of the molecule

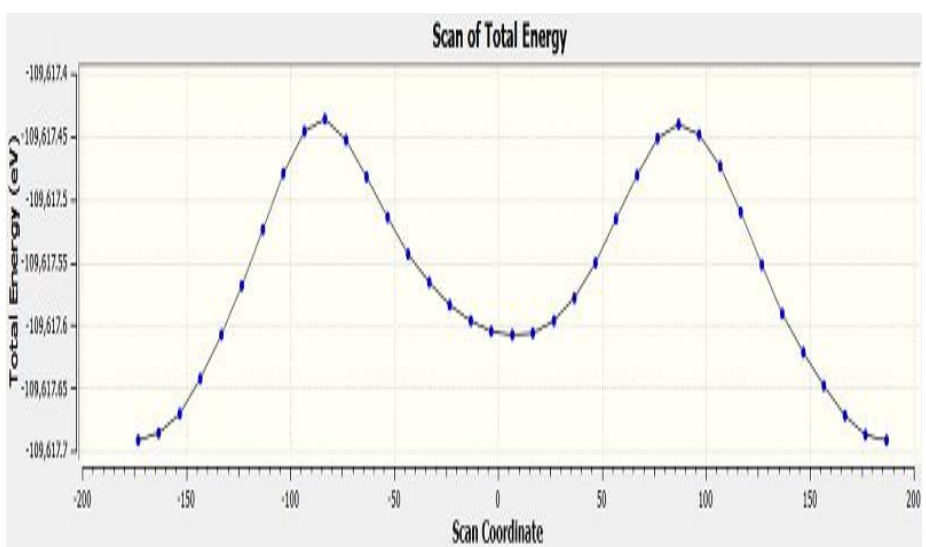


Figure 3. Energy versus dihedral angle of BPTO.

## **3.1.2** Vibrational Frequency Analysis and Structural Correlation:

The optimized molecular geometry of 2-(5-bromo-2-(trifluoromethoxy)phenyl)-<math>5-(thiophen-2-yl)-

1,3,4-oxadiazole was validated through vibrational frequency analysis, with key assignments presented in Table 2. The IR frequencies are in good agreement with the expected stretching and deformation modes based on DFT calculations. Characteristic C-H stretching vibrations appear in the region 3224-3267 cm<sup>-1</sup>, attributed to various hydrogen atoms across the phenyl, thiophene, and oxadiazole rings. Specifically, the strong peaks at 3242, 3267, and 3241 cm<sup>-1</sup> correspond to the νC7νC11–H13, and vC16-H19 respectively, indicating intact aromatic C-H bonds. The C=N stretching vibrations are observed around 1631 cm<sup>-1</sup> (vN4-C1 and vC6-C7) and 1573 cm<sup>-1</sup> (vN5-C3), aligning well with typical oxadiazole ring vibrations. These values reflect the presence of delocalized electron density in the heterocyclic core and are consistent with the computed bond length of ~1.31 Å, slightly shorter than the experimental XRD values (1.364–1.373 Å) <sup>28</sup>. The C–O and C–F modes associated stretching with trifluoromethoxy group are seen at 1248 cm-1 (vO23-C25, vF28-C25), 1290 cm<sup>-1</sup> (vF26-C25) and 1215 cm<sup>-1</sup> (vF27-C25). These values confirm the strong electron-withdrawing character of the -OCF<sub>3</sub> group, which contributes to elongation of adjacent bonds like C14-C15 and C14-C16 (1.4014 Å and 1.4098 Å), as noted in the geometry analysis as Red shift hydrogen bonding. C-Br stretching vibrations are assigned at 387 cm<sup>-1</sup> and 252 cm<sup>-1</sup>, confirming the presence of the halogen substituent. Modes involving the thiophene ring are observed at 752 cm<sup>-1</sup> and 863 cm<sup>-1</sup>, assigned to vS8-C11 and associated bending modes.

The coupling of stretching and deformation modes, such as δH10–C7–C9 and δH13–C11–S8, observed in the 1340-1500 cm<sup>-1</sup> range, provides further support for the structural integrity and connectivity of the rings. Low-frequency torsional modes  $(\tau)$ below 1000 cm<sup>-1</sup> such as 944, 942, and 975 cm<sup>-1</sup> reflect internal rotations and twisting between rings, especially notable in the large dihedral angle (82.66°) between the trifluoromethoxy group and the phenyl ring<sup>29</sup>. In the investigated molecule, a correlation is observed between the shortening of C-H bond lengths and an increase in their stretching vibrational frequencies. The relatively higher frequency of the C11-H13 stretching mode suggests a shorter and stronger bond compared to the others. This is consistent with the principle that shorter bonds exhibit higher bond force constants, which translates to increased vibrational frequencies in IR spectra. These increased vibrational frequencies are expected and foreseen in Geometrical optimization studies due to Blue Shift hydrogen bonding 30-31. Conversely, modes such as C7-H10 and C20-H22 show slightly lower frequencies (comparatively), indicating

comparatively longer bond lengths or greater electron delocalization in their local environments which is possibly due to conjugative effects or the influence of nearby electronegative substituents. Thus, the vibrational frequency trends align well with the calculated bond lengths, reinforcing the inverse relationship between bond length and stretching frequency in harmonic oscillator terms. This highlights the sensitivity of vibrational spectroscopy to subtle electronic and structural variations within the molecule.Overall, vibrational profile confirms the stability of the optimized structure and complements the bond length analysis, substantiating the presence and orientation of key functional groups within the molecule.

## 3.1.3 <sup>1</sup>H and <sup>13</sup>C NMR Spectral Analysis and Hydrogen Bonding Effects:

The <sup>1</sup>H and <sup>13</sup>C NMR spectral data of 2-(5-bromo-2-(trifluoromethoxy)phenyl)-5-(thiophen-2-yl)-1,3,4-oxadiazole (BPTO) are summarized in Table 3. In the <sup>1</sup>H NMR spectrum, aromatic proton signals appear in the range of 7.98 to 9.64 ppm, characteristic of deshielded aromatic environments. The H19 proton resonates downfield at 9.64 ppm, which is attributed to the strong electronwithdrawing effect of the adjacent Br24 atom. In intramolecular BPTO, potential hvdrogen bonding involving heteroatoms such as oxygen (O2, O23) and nitrogen (N4, N5) may contribute to these shifts. For instance, if H19 is engaged in a red-shifted hydrogen bond with a nearby electronegative atom, this could explain its pronounced downfield signal at 9.64 ppm. The <sup>13</sup>C NMR spectrum reveals 13 distinct signals, consistent with chemically non-equivalent carbon environments. The C14 and C17 signals are observed upfield, due to  $\pi$ -conjugation with the oxygen atom (O23). In this context, the electrondonating resonance effect of the oxygen dominates over its inductive withdrawal, leading to increased shielding. Carbons C7 and C9 also appear in the upfield region, due to the moderate inductive effect of the thiophene sulfur (S8), which is less electronegative compared to oxygen or fluorine. In contrast, C25 appears downfield, a result of the strong electron-withdrawing effect of the trifluoromethyl group (-CF<sub>3</sub>). This deshielding arises due to the significant reduction in electron density around C25. The C1 and C3 carbons, adjacent to O2, N4, and N5, show downfield chemical shifts at 165 and 164 ppm, respectively. These shifts reflect the cumulative electron-withdrawing effects of the surrounding heteroatoms, particularly in the oxadiazole ring system 32-33.

Table 3. <sup>1</sup>H and <sup>13</sup>C NMR spectral analysis of BPTO

Position of H atom	Observed values (ppm)	Position of C atom	Observed values (ppm)
19-H	9.64	1-C	165.80
10-H	8.75	3-C	164.77
13-H	8.28	15-C	149.62
22-H	8.27	18-C	145.80
21-H	8.25	11-C	139.26
12-H	7.98	6-C	137.70
		20-C	137.40
		16-C	136.72
		25-C	134.10
		7-C	132.87
		9-C	129.14
		17-C	129.08
		14-C	127.30

#### 3.1.4 NBO analysis:

The NBO study was performed using Gaussian 09, DFT B3LYP6-311G(d,p). The NBO is an effective study for chemical interpretation of hyperconjugate interaction and electron density movement from filled lone pair electrons. The aim of NBO analysis is to predict donor orbitals, acceptor orbitals, and interaction stabilisation energy, which is a result of second order perturbation theory. The most valuable interactions between donor and acceptor are reported in Table 4. It is known that larger E(2)s represent intensive interaction between donor and acceptor. E(2) also proves the efficacy of

conjugation in the molecule. There is more interaction, which stabiles the molecule. Pronounceable interactions are  $\pi$ - $\sigma$ \*, LP- $\sigma$ \* which are indicative of Blue shift hydrogen bonding [34]. The interactions presented in Table 4 are evident for Blue shift hydrogen bonding, where the LP electrons are pushed into the sigma anti bonding orbital of the acceptor. The electron push increases the bond order decreases the bond length and increases the vibrational frequency. These features have been discussed in Geometry optimization, Vibrational frequency and it is also confirmed by the low E2 values.

Table 4. NBO analysis of BPTO

Donor	Acceptor	E(2)	E(j)-E(i)	F(i,j)
		kcal/mo	a.u.	a.u.
π-C1-N4	π*-C3-N5	12.04	0.33	0.059
π-C3-N5	π*-C1-N4	10.42	0.34	0.055
π-C3-N5	π*-C14-C15	9.95	0.34	0.056
π-C6-C7	π*-C1-N4	22.02	0.28	0.072
σ-C6-C7	π*-C9-C11	15.29	0.29	0.061
π-C9-C11	π*-C6-C7	16.58	0.29	0.065
π-C14-C15	π*-C3-N5	18	0.28	0.064
π-C14-C15	π*-C16-C18	19.88	0.29	0.068
π-C14-C15	π*-C17-C20	19.37	0.3	0.068
π-C16-C18	π*-C14-C15	17.92	0.28	0.065
σ-C16-C18	π*-C17-C20	20.13	0.29	0.069
π-C17-C20	π*-C14-C15	21.76	0.27	0.07
σ-C17-H20	π*-C16-C18	19.29	0.28	0.065
LP (2) O2	π*-C1-N4	34.29	0.36	0.099
LP(1)O2	π*-C3-C5	34.24	0.35	0.098
LP(1) N4	σ*-C1-O2	11.03	0.73	0.08
LP (1) N5	σ*-O2-C3	10.86	0.72	0.079
LP(2) S8	π*-C6-C7	21.54	0.26	0.068
LP(1)S8	π*-C9-C11	22.58	0.26	0.07
LP (2) O23	σ*-C25-F27	14.79	0.56	0.082
LP (1) O23	σ*-C25-F28	13.57	0.57	0.079
LP (1) Br24	π*-C16-C18	10.1	0.3	0.053
LP (2) F26	σ*-O23-C25	11.98	0.73	0.084
LP (3) F26	σ*-C25-F27	10.99	0.64	0.076
LP (1) F26	σ*-C25-F28	12.39	0.65	0.081
LP (2) F27	σ*-O23-C25	11.28	0.73	0.082
LP (3) F27	σ*-C25-F26	14.71	0.65	0.089
LP (2) F27	σ*-O23-C25	11.71	0.73	0.083
LP (3) F28	σ*-C25-F26	15.15	0.66	0.09

This analysis revealed several notable  $\sigma \to \sigma^*$  and  $\sigma \to \pi^*$  interactions. Among them, the  $\sigma(C-H) \to$  $\sigma(C-C)^*$  interaction from the donor bond C17–H21 into the antibonding orbital of C18-C20 exhibited a stabilization energy E(2) = 3.91 kcal/mol, indicating a significant classical hyperconjugative effect. Similarly, the σ(C18-C20) bond showed delocalization into various neighboring antibonding orbitals such as C16-C18, C17-C20, and C20-H22, with E(2) values ranging from 2.17 to 4.16 kcal/mol, suggesting a strongly conjugated σframework in this region. Notably, hyperconjugation involving halogen substituents was observed. The  $\sigma(C18\text{-Br}24) \rightarrow \sigma(C14\text{-C}16)^*$ interaction contributed E(2) = 3.38 kcal/mol, highlighting the role of the bromine substituent in modulating the electronic environment via delocalization into the aromatic system.

Such halogen-involved hyperconjugation is known to impact molecular polarizability and reactivity in substituted aryl compounds. Furthermore, the

 $\sigma(C1-O2) \rightarrow \sigma(C3-C14)^*$  and  $\sigma(C1-O2) \rightarrow \sigma(C6-C1)^*$ S8)\* interactions provided additional stabilization energies of 4.32 and 4.66 kcal/mol, respectively. Though traditionally attributed to lone pair interactions (n  $\rightarrow \sigma^*$ ), the orbital occupancy analysis supports a σ-donating character consistent hyperconjugation in a conjugated heteroatomic system. These interactions collectively contribute to the delocalized electronic character of molecule, the affecting conformational preference, aromaticity, potential reactivity.

#### 3.1.5 Molecular Orbital Visualization:

The highest occupied molecular orbital (HOMO) and lowest unoccupied molecular orbital (LUMO) are shown in **Figure 3** and **Figure 4**. The HOMO is primarily localized over the aromatic and heteroaromatic core, indicating potential donor sites, while the LUMO is distributed across the acceptor substituents, consistent with intramolecular charge transfer behavior.

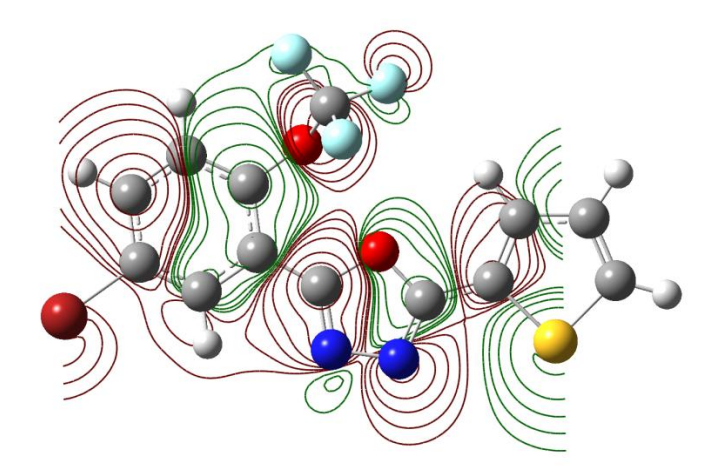


Figure 4: HOMO orbital surface of the molecule showing delocalization over the aromatic framework.

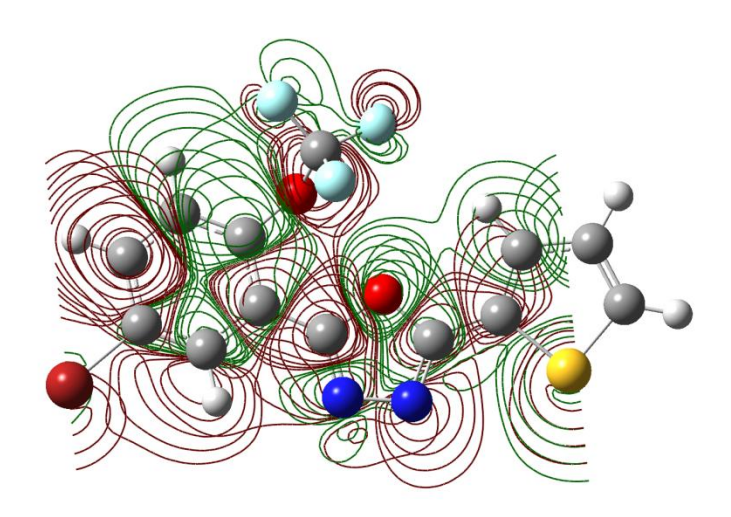


Figure 5: LUMO orbital surface localized on electron-withdrawing groups, suggesting acceptor character.

Table 5. Electronic and Global descriptors of BPTO

Table 5. Electronic and Giobai des	criptors of Br 10
Descriptor	Value (eV)
Еномо	-5.7019
ELUMO	-2.4508
Energy Gap (ΔE)	3.2511
Ionization Potential (IP)	5.7019
Electron Affinity (EA)	2.4508
Electronegativity (χ)	4.0763
Chemical Potential (µ)	-4.0763
Hardness (η)	1.6256
Electrophilicity (ω)	5.1110

As shown in **Figure 5**, the HOMO orbitals are primarily localized over the thiophene ring, imidazole ring, and partially on the phenyl moiety, while the LUMO is concentrated on the phenyl and imidazole units. The small HOMO-LUMO gap ( $\Delta E = 3.2511 \text{ eV}$ ) suggests that the molecule is likely to undergo electronic transitions, indicating possible optical activity and polarizability [34]. A smaller gap correlates with increased softness and polarizability. These values reflect that the compound is chemically hard with good kinetic stability, strong electrophilicity, and a good balance of donor/acceptor character. The high ionization potential (compared to electron affinity) further supports its electron-donating ability.

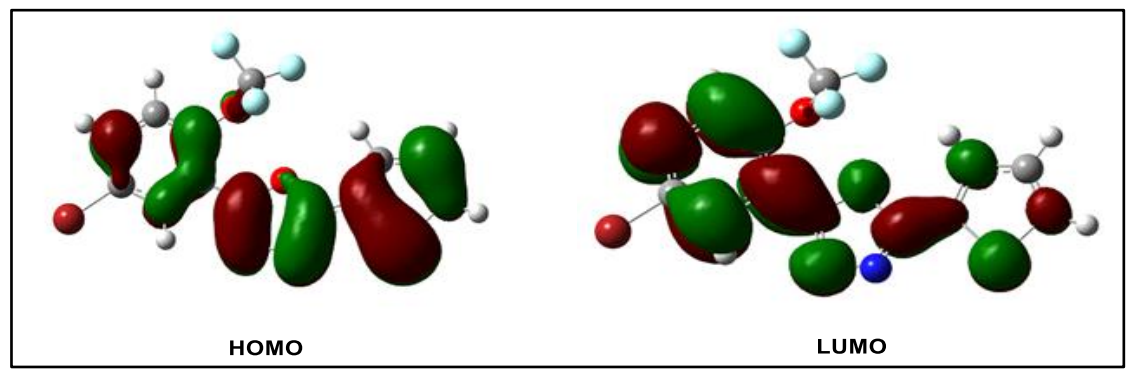


Figure 6. HOMO-LUMO diagrams of BPTO

## 3.1.6 NLO Properties of BPTO

Nonlinear optical (NLO) studies have attracted increasing interest due to their role in optical switching, modulation, logic and memory that are key elements in emerging fields such as signal processing, telecommunications, and optical computing. For the studied compound (BPTO), the NLO parameters were calculated at the DFT level and compared against reference values for urea, a standard benchmark for NLO performance. **Table 6** reveals that when compared to urea ( $\mu = 1.3732$  Debye,  $\beta = 3.7289 \times 10^{-31}$  esu), the title compound exhibits a significantly higher dipole moment and hyperpolarizability, indicating stronger NLO response.

Table 6. NLO calculation of BPTO

Table 6. NEO calculation of DI 10							
Dipole me	oment	Hyperpolarizability					
$\mu_{x}$	1.0031	$\beta_{xxx}$	24.0615				
$\mu_{\mathrm{y}}$	3.3194	$\beta_{yyy}$	58.1471				
μz	-0.3519	$\beta_{zzz}$	15.3104				
μ	3.4855	$\beta_{xyy}$	-62.8493				
(Debye)							
Polarizab	ility	$\beta_{xxy}$	21.3683				

$\alpha_{xx}$	-113.92	$\beta_{xxz}$	3.4726
$\alpha_{YY}$	-146.98	$\beta_{xzz}$	-52.3373
$\alpha_{ZZ}$	-142.71	$\beta_{yzz}$	8.574
$\alpha_{XY}$	-2.02	$\beta_{yyz}$	1.7057
$\alpha_{YZ}$	1.28	$\beta_{xyz}$	4.6525
$\alpha_{yz}$	-1.25	$\beta_{tot}$	128.3874
$\alpha_0$	-1.993	$\beta_0$	1.109
		$(10^{-30}$	
		esu)	
$\alpha_{\mathrm{tot}}$	4.353		
$(10^{-30}$			
esu)			

Thus, BPTO is a promising candidate for NLO applications, especially where higher molecular responsiveness is essential.[35-37]

#### 3.1.7 Charge Distribution Analysis:

Charge distribution over atoms provides essential insights into the electronic structure, polarity, and reactive behavior of molecules. Both Mulliken and Natural Bond Orbital (NBO) analyses were employed to assess the charge delocalization in the titled compound. The Mulliken atomic charges (Figure 6) reveal that heteroatoms like oxygen and nitrogen bear significant negative charges, consistent with their electronegativity. Oxygen

atom  $O_2$  is highly negative, suggesting its potential as a strong nucleophilic site and its involvement in intramolecular interactions such as hydrogen bonding. Similarly, nitrogen atoms  $N_4$  and  $N_5$  exhibit negative charge accumulation, indicating their role in  $\pi$ -delocalization and resonance stabilization within the conjugated system. The NBO charge distribution (Figure 7) offers a more refined description, accounting for natural atomic orbitals and bonding interactions. Here, the electron density localization is slightly shifted compared to Mulliken analysis, but consistent trends are observed as oxygen and nitrogen atoms retain higher electron density, whereas hydrogen atoms

show positive values, supporting their role in polar interactions. The comparison between Mulliken and NBO charges highlights the robustness of electron localization on electronegative centers. supports the NBO second-order perturbation analysis, which shows lone pair to antibonding orbital interactions, especially from oxygen and nitrogen donors, leading to stabilization energies (E2) as high as ~34 kcal/mol. These charge distribution patterns are also corroborated by Fukui function values and MEP mapping, further pinpointing the reactive nucleophilic and electrophilic regions across the molecular surface.

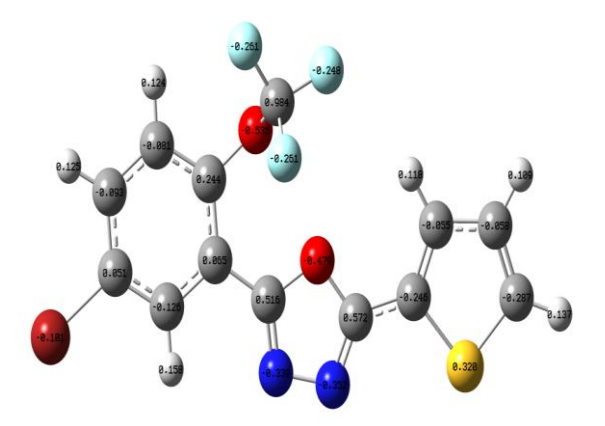


Figure 7. Mulliken Atomic Charges

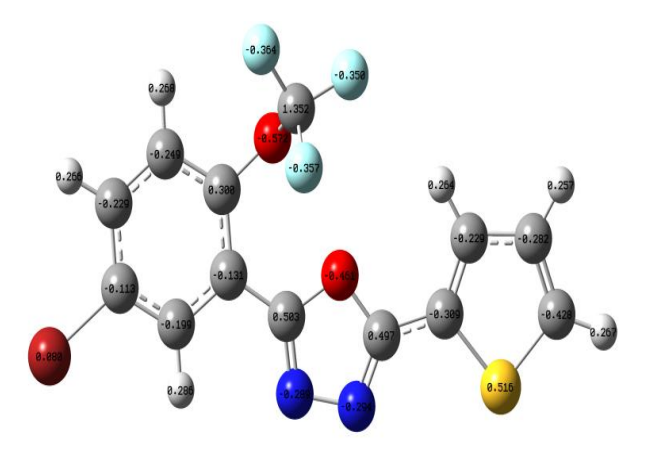


Figure 8. NBO Charges disatribution

### 3.1.8 HOMA analysis:

Aromaticity of titled compound is determined by theoretically by expansion of HOMA. The values are listed in **Table 7** and this model is based on the following equation (ii).

HOMA = 
$$1 - \left[ \left( \frac{\alpha}{n} \sum R_{opt} - R_i \right)^2 \right]$$
  
=  $1 - \alpha (R_{opt} - R_i)^2 - \left( \frac{\alpha}{n} \right) \sum (R_{av} - R_i)^2$ 

where  $\alpha$  ( ie = 257.7) is an empirical constant that is fixed so that aromatic compounds (where all bonds equal  $R_{opt}$  =1.388) and Ri is the individual bond lengths. Since both the EN and GEO terms are dearomatization terms, an increase or decreases in either term the degree of aromaticity. EN terms the difference between the mean bond length and

the optimal bond length, and the GEO terms the degree of bond alternation. The bond lengths used in this calculation can be computed or measured experimentally. The aromaticity of the phenyl bromide ring was evaluated using the HOMA model. The calculated HOMA value of **0.9360** is close to the reference benzene value (0.982), indicating significant aromatic character.<sup>38</sup>.

3.1.9 Fuki Function:

Table 7. Calculated local reactivity properties BPTO

Atoms	f <sub>cat</sub> +=A-N	f <sub>anion</sub> =N-C	S+=sf+	S-=sf-	ΔS=S+(- )S-	Sk+/sk-	ω+=ωf+	ω-=ωf-	Δω(ω+(- )ω-)
C1	-0.044	-0.035	-0.016	-0.012	-0.003	1.260	-0.744	-0.591	-0.154
O2	-0.030	-0.016	-0.011	-0.006	-0.005	1.929	-0.505	-0.262	-0.243
C3	-0.056	-0.049	-0.020	-0.017	-0.003	1.149	-0.940	-0.819	-0.122
N4	-0.043	-0.066	-0.015	-0.023	0.008	0.650	-0.716	-1.102	0.386
N5	-0.053	-0.051	-0.019	-0.018	-0.001	1.037	-0.892	-0.860	-0.032
C6	0.001	-0.023	0.000	-0.008	0.008	-0.025	0.009	-0.383	0.393
C7	-0.036	-0.032	-0.013	-0.011	-0.001	1.127	-0.609	-0.540	-0.068
S8	-0.114	-0.127	-0.040	-0.045	0.005	0.892	-1.907	-2.138	0.232
C9	-0.003	-0.019	-0.001	-0.007	0.005	0.180	-0.057	-0.316	0.260
C11	-0.027	-0.046	-0.010	-0.016	0.007	0.582	-0.453	-0.779	0.326
C14	-0.018	0.000	-0.007	1.244	-0.006	-554.909	-0.307	0.001	-0.308
C15	-0.036	-0.033	-0.013	-0.012	-0.001	1.083	-0.605	-0.559	-0.046
C16	-0.032	-0.018	-0.011	-0.006	-0.005	1.782	-0.543	-0.305	-0.238
C17	-0.010	-0.009	-0.004	-0.003	0.000	1.076	-0.168	-0.156	-0.012
C18	0.008	0.011	0.003	0.004	-0.001	0.737	0.141	0.191	-0.050
C20	-0.051	-0.034	-0.018	-0.012	-0.006	1.506	-0.857	-0.569	-0.288
O23	-0.005	-0.007	-0.002	-0.003	0.001	0.655	-0.080	-0.122	0.042
Br24	-0.104	-0.121	-0.037	-0.043	0.006	0.857	-1.747	-2.039	0.292
C25	-0.010	-0.007	-0.004	-0.003	-0.001	1.422	-0.167	-0.118	-0.050
F26	-0.009	-0.005	-0.003	-0.002	-0.001	1.832	-0.152	-0.083	-0.069
F27	-0.016	-0.016	-0.006	-0.006	0.000	1.002	-0.273	-0.273	0.000
F28	-0.004	-0.003	-0.001	-0.001	0.000	1.131	-0.064	-0.057	-0.007

Fukui functions provide insight into the regioselectivity and reactivity of individual atoms in a molecule. Sites with large **fk**+ values are prone to nucleophilic attack, whereas sites with high fkare susceptible to **electrophilic attack**. The trends from the calculated descriptors shows nucleophilic **reactivity order** of C18 > C6 > C9 > F28 > O23 >F26 > C17 > C25 and electrophilic reactivity **order of** C18 > C14 > F28 > F26 > C25 > O23. Notably, C18 acts both as a donor and acceptor but is 1.3× more prone to accept electrons. S8 also serves as both, with a greater tendency as an electron donor. The local electrophilicity ratio (sk+/sk-) is lowest for C14, indicating it acts mainly as an electron donor, while O2 displays the highest ratio, making it a strong electron acceptor<sup>39</sup>.

## 3.1.10 Nucleus Independent Chemical Shift (NICS) Analysis:

The aromaticity of the studied reveals that the BPTO molecule contains, one thiophene ring, a five-membered ring, and a phenyl ring which was evaluated using the Nucleus Independent Chemical Shift (NICS) method. NICS values displayed in **Table 8** were computed at various distances along

Table 8. Nucleus Independent Chemical Shifts of BPTO

the perpendicular axis (z-axis) ranging from -2.0 Å to +2.0 Å at increments of 0.5 Å. Both isotropic and anisotropic shielding values were calculated using the GIAO method at the B3LYP/6-311+G(d,p) level of theory, in accordance with established protocols for evaluating magnetic aromaticity indicators. The isotropic NICS values provide an estimate of the magnetic shielding experienced at a given point in space near the ring. A more negative NICS value indicates a diatropic ring current, typical of aromatic systems, whereas positive values or values close to zero suggest nonaromatic or antiaromatic character. The anisotropic values offer further insight into  $\pi$ -electron delocalization and the out-of-plane magnetic shielding components (NICS(zz)). The thiophene ring displayed isotropic NICS values increasing z = -2.0 Å to a maximumfrom -1.1265 at of 12.0509 at the ring center (z = 0 Å). This trend, with the most negative value slightly below the ring plane and positive values near the ring center, is characteristic of a modestly aromatic heterocycle. The anisotropic shielding peaked at 22.6079 (z = -1 Å), highlighting strong  $\pi$ -electron circulation perpendicular to the ring plane.

Bq	Thiopene ring		Five Men	Five Membered ring		n ring
	Isotropic	Anisotropic	Isotropic	Anisotropic	Isotropic	Anisotropic
-2	-1.1265	14.1319	0.2119	10.1007	0.178	16.4294
-1.5	-0.4861	19.9425	1.7958	15.107	2.9394	21.7138
-1	2.2654	22.6079	5.0854	18.7999	7.2856	21.1522
-0.5	7.3195	12.6599	7.6364	8.3742	10.7126	11.5812
0	12.0509	1.2811	7.2033	-4.6782	11.049	9.9476
0.5	7.3195	12.6599	9.1019	11.6341	8.0554	18.8494
1	7.3195	12.6599	5.7851	18.6209	4.0352	20.6314
1.5	7.3195	12.6599	2.1774	14.0659	1.2435	15.8835
2	7.3195	12.6599	0.4698	9.339	0.0382	10.9582

For the five-membered ring, the NICS values varied from 0.2119 (z = -2.0 Å) to a maximum of 9.1019 (z = +0.5 Å), suggesting mild aromatic character but notably lower than that observed in the thiophene ring. The anisotropic values followed a similar trend, peaking at 18.7999 (z = -1 Å), reinforcing moderate  $\pi$ -delocalization. The main ring exhibited the highest anisotropic shielding values among the three systems, with a maximum of 21.7138 at z = -1.5 Å and a substantial isotropic minimum of 0.0382 at z = +2.0 Å. These findings suggest the main ring has a stronger aromatic or pseudoaromatic character, likely influenced by electronic effects from attached substituents. The sharp change in anisotropic values around  $z = \pm 1 \text{ Å}$ indicates significant out-of-plane electron delocalization, which is characteristic of enhanced conjugation. Comparing all three ring systems, it is evident that the phenyl ring exhibits the most pronounced anisotropic shielding, signifying a higher degree of aromaticity. The thiophene ring, although aromatic, is moderately less so, whereas the five-membered ring shows the lowest aromatic response. These observations align well with their respective electronic structures and substituent effects<sup>40,41</sup>.

### 3.2 Molecular Docking study of BPTO:

Molecular docking analysis was used to examine the binding affinity and interactions <sup>42</sup> between the ligand and the target protein 6XXO. The docking

data indicated a reasonably strong contact between the ligand and the 6XXO active site, which showed a binding energy of -6.6 kcal/mol. The docking pose visualization (Figure 8) clearly shows that the ligand is properly positioned within the active site and forms important interactions with important amino acid residues. The stability of the ligand within the binding pocket may be attributed to its hydrogen bonding with residues like SER-108. Hydrophobic interactions and  $\pi$ - $\pi$  stacking with aromatic residues further increase ligand affinity <sup>43,44</sup>. The ligand's binding orientation is stabilized by the protein's secondary structure, which comprises  $\alpha$ -helices and  $\beta$ -sheets. The existence of non-covalent interactions, such as van der Waals forces and electrostatic interactions influences the overall stability of the ligand-protein.

The docking score of -6.6 kcal/mol indicates a modest binding affinity, which can be further adjusted by changing the ligand's structure to improve its interaction with the binding site. Future research, such as molecular dynamics simulations, may shed more light on the ligand-protein complex's conformational stability and possible biological activity. This docking research is the first stage in assessing the ligand's therapeutic potential against the target protein 6XXO which is associated with prostate cancer. Further experimental validation, such as in vitro binding assays, will be necessary to confirm the omputational predictions.



Figure 8. Docking pose of BPTO with 6XXO protein

#### 4. CONCLUSIONS:

Theoretical investigations of the target compound, carried out via DFT and NBO frameworks, have provided profound insights into its structural and attributes. The **NBO** electronic analysis underscored substantial donor-acceptor interactions, with strong hyperconjugative effects stabilizing the molecule. The HOMO-LUMO gap of 3.2511 eV, along with high global hardness and electrophilicity values, indicates considerable kinetic stability and a moderate reactivity profile. Nonlinear optical calculations reveal promising optical behavior, with  $\beta_0$  values on par with urea, supporting its potential use in optoelectronic devices. Aromaticity indices and MEP surface analysis corroborated the existence of reactive  $\pi$ electron regions and charge-rich zones, while Fukui descriptors identified electrophilic and nucleophilic centers, facilitating a deeper understanding of potential reaction mechanisms. Collectively, these computational insights establish the compound as a chemically robust system with prospective applications in optical switching, drug design, and electronic materials.

#### **Author Contributions:**

The manuscript was written through contributions of all authors. All authors have given approval to the final version of the manuscript. CRediT: Savarivappan Albert Nikson methodology, software, formal analysis, data curation, writing original draft; Richard Rajkumar Siluvairaj methodology, software, formal analysis, data curation, writing - original draft; David Amalraj Savarimuthu data curation, formal analysis, writing - original draft; T. Antony Sandosh writing – original draft, data curation; **Chinnappan Adaikalaraj** writing – original draft, data curation; Manivarman review & editing, conceptualization, investigation, supervision.

#### **ACKNOWLEDGMENTS:**

Authors thank St. Joseph's College of Arts and Science (Autonomous), Cuddalore-1 for providing Chemistry Research Laboratory facilities and also thank PG and Research Department of Chemistry, Government Arts College, C-Mutlur, Chidambaram, for providing infrastructure facilities.

## **CONFLICTS OF INTEREST:**

The authors declare no conflict of interest.

### **REFERENCE:**

1. Boström, J., Hogner, A., Llinàs, A., Wellner, E., &

- Plowright, A. T. (2012). Oxadiazoles in Medicinal Chemistry. Journal of Medicinal Chemistry, 55(5), 1817–1830. https://doi.org/10.1021/jm2013248
- 2 Patani, G. A., & LaVoie, E. J. (1996). Bioisosterism: A Rational Approach in Drug Design. Chemical Reviews, 96(8), 3147–3176. https://doi.org/10.1021/cr950066q
- 3 Kadi, A. A., El-Brollosy, N. R., Al-Deeb, O. A., Habib, E.-S. E., Ibrahim, T., & El-Emam, A. A. (2007). Synthesis, antimicrobial, and anti-inflammatory activities of novel 2-(1-adamantyl)-5-substituted-1,3,4-oxadiazoles and 2-(1-adamantylamino)-5-substituted-1,3,4-thiadiazoles. 42(2), 235–242. https://doi.org/10.1016/j.ejmech.2006.10.003
- 4 Palaska, E., Şahin, G., Kelicen, P., Durlu, N. Tuğba., & Altinok, G. (2002). Synthesis and anti-inflammatory activity of 1-acylthiosemicarbazides, 1,3,4-oxadiazoles, 1,3,4-thiadiazoles and 1,2,4-triazole-3-thiones. II Farmaco, 57(2), 101–107. https://doi.org/10.1016/s0014-827x(01)01176-4
- 5 Alisi, I. O., Uzairu, A., & Abechi, S. E. (2020). Free radical scavenging mechanism of 1,3,4-oxadiazole derivatives: thermodynamics of O–H and N–H bond cleavage. Heliyon, 6(3), e03683. https://doi.org/10.1016/j.heliyon.2020.e03683
- 6 Savarino, A. (2006). A historical sketch of the discovery and development of HIV-1 integrase inhibitors. Expert Opinion on Investigational Drugs, 15(12), 1507–1522. https://doi.org/10.1517/13543784.15.12.1507
- 7 James, N. D., & Growcott, J. W. (2009). Zibotentan endothelin ETA receptor antagonist oncolytic. Drugs of the Future, 34(8), 624. https://doi.org/10.1358/dof.2009.34.8.1400202
- 8 Adelstein, G. W., Yen, C. H., Dajani, E. Z., & Bianchi, R. G. (1976). 3,3-Diphenyl-3-(2-alkyl-1,3,4-oxadiazol-5-yl)propylcycloalkylamines, a novel series of antidiarrheal agents. Journal of Medicinal Chemistry, 19(10), 1221–1225. https://doi.org/10.1021/jm00232a010
- 9 Ducharme, Y., Blouin, M., Brideau, C., Châteauneuf, A., Gareau, Y., Grimm, E. L., Hélène Jûteau, Sébastien Laliberté, Mackay, B., Fréderic Massé, Ouellet, M., Salem, M., Styhler, A., & Friesen, R. W. (2010). The Discovery of Setileuton, a Potent and Selective 5-Lipoxygenase Inhibitor. ACS Medicinal Chemistry Letters, 1(4), 170– 174. https://doi.org/10.1021/ml100029k
- 10. 10 Barbarella, G., Zangoli, M., & Di Maria, F. (2017). Synthesis and Applications of Thiophene Derivatives as Organic Materials. Advances in Heterocyclic Chemistry, 105–167. https://doi.org/10.1016/bs.aihch.2017.01.001
- Dalvie, D. K., Kalgutkar, A. S., Khojasteh-Bakht, S. C., Obach, R. S., & O'Donnell, J. P. (2002).
  Biotransformation Reactions of Five-Membered Aromatic Heterocyclic Rings. Chemical Research in Toxicology, 15(3), 269–299. https://doi.org/10.1021/tx015574b
- 12 Eustáquio, A. S., O'Hagan, D., & Moore, B. S. (2010). Engineering Fluorometabolite Production: Fluorinase Expression in Salinispora tropica Yields Fluorosalinosporamide. Journal of Natural Products, 73(3), 378–382. https://doi.org/10.1021/np900719u
- 13 Bhattacharya, S., Biswas, C., Sai, Krishna, Devulapally Koteshwar, Lingamallu Giribabu, & Rao, S. V. (2019). Optoelectronic, femtosecond nonlinear optical properties and excited state dynamics of a triphenyl imidazole induced phthalocyanine derivative. RSC Advances, 9(63), 36726–36741. https://doi.org/10.1039/c9ra07758h
- 14 Vineetha, P. K., A. Aswathy, E. Shiju, K. Chandrasekharan, & N. Manoj. (2020). Structure–property correlations of the nonlinear optical properties of a few bipodal D–π–A molecules an experimental and theoretical approach. New Journal of Chemistry, 44(16), 6142–6150. https://doi.org/10.1039/c9nj06344g
- 15. 15 Prakasam, M., & Anbarasan, P. M. (2016). Second order hyperpolarizability of triphenylamine based organic sensitizers: a first principle theoretical study. RSC

- Advances, 6(79), 75242–75250. https://doi.org/10.1039/c6ra11200e
- Almeida, L., Anjos, M. M., Ribeiro, G., Valverde, C., Daniel Aragão Machado, Oliveira, G., Napolitano, H. B., & de, B. (2017). Synthesis, structural characterization and computational study of a novel amino chalcone: a potential nonlinear optical material. New Journal of Chemistry, 41(4), 1744–1754. https://doi.org/10.1039/c5nj03214h
- 17 Bhardwaj, N., Saraf, S. K., Sharma, P., & Kumar, P. (2009). Syntheses, Evaluation and Characterization of Some 1, 3, 4-Oxadiazoles as Antimicrobial Agents. E-Journal of Chemistry, 6(4), 1133–1138. https://doi.org/10.1155/2009/698023
- Deshapande, N., Belavagi, N. S., Sunagar, M. G., Gaonkar, S., Pujar, G. H., Wari, M. N., Inamdar, S. R., & Khazi, I. A. M. (2015). Synthesis, characterization and optoelectronic investigations of bithiophene substituted 1,3,4-oxadiazole derivatives as green fluorescent materials. RSC Advances, 5(105), 86685–86696. https://doi.org/10.1039/C5RA14550C
- 19 Liu, S., Wu, Q., Zhang, T., Zhang, H., & Han, J. (2021). Supramolecular brush polymers prepared from 1,3,4-oxadiazole and cyanobutoxy functionalised pillar[5]arene for detecting Cu2+. Organic & Biomolecular Chemistry, 19(6), 1287–1291. https://doi.org/10.1039/D0OB02587A
- Westphal, E., Gallardo, H., Sebastián, N., Eremin, A., Prehm, M., Alaasar, M., & Tschierske, C. (2019). Liquid crystalline self-assembly of 2,5-diphenyl-1,3,4-oxadiazole based bent-core molecules and the influence of carbosilane end-groups. Journal of Materials Chemistry C, 7(10), 3064–3081. https://doi.org/10.1039/c8tc06591h
- 21 Paun, A., Hadade, N. D., Paraschivescu, C. C., & Matache, M. (2016). 1,3,4-Oxadiazoles as luminescent materials for organic light emitting diodes via crosscoupling reactions. Journal of Materials Chemistry C, 4(37), 8596–8610. https://doi.org/10.1039/c6tc03003c
- 22. Rababa, M. H., Alsaleh, M. M., Abusamhadaneh, A. A., Younes, E. A., Natsheh, I. Y., & Rasras, A. J. (2023). Synthesis, Biological Activity and DFT Studies of 1,3,4-oxadiazole Ring in Combination with Pyridinium Salt. Current Organic Chemistry, 27(1), 62–70. https://doi.org/10.2174/1385272827666230227120641
- 23 Mickevičius, V., Vaickelionienė, R., & Sapijanskaitė,
  B. (2009). Synthesis of substituted 1,3,4-oxadiazole derivatives. Chemistry of Heterocyclic Compounds, 45(2), 215–218. https://doi.org/10.1007/s10593-009-0252-4
- 24 Rauhut, G., & Pulay, P. (1995). Transferable Scaling Factors for Density Functional Derived Vibrational Force Fields. The Journal of Physical Chemistry, 99(10), 3093– 3100. https://doi.org/10.1021/j100010a019
- 25 Scott, A. P., & Radom, L. (1996). Harmonic Vibrational Frequencies: An Evaluation of Hartree–Fock, Møller–Plesset, Quadratic Configuration Interaction, Density Functional Theory, and Semiempirical Scale Factors. The Journal of Physical Chemistry, 100(41), 16502–16513. https://doi.org/10.1021/jp960976r
- 26 Frisch, M., Trucks, Gary., Schlegel, H., Scuceria, G., & Robb, Michael., Cheeseman, James., & Pople, J.. (2003). Gaussian 03, revision A.1; Gaussian, Inc.: Pittsburg, PA, 2003.
- 27 Michal. H. Jamróz, Vibrational Energy Distribution Analysis VEDA 4, Warsaw, 2004-2010, https://smmg.pl/software/veda
- 28 Fatmah A. M. Al-Omary, Olivier Blacque, Alanazi, F. S., Edward, & El-Emam, A. A. (2023). Crystal structure of 2-[(4-bromobenzyl)thio]-5-(5-bromothiophen-2-yl)-1,3,4-oxadiazole, C13H8Br2N2OS2. Zeitschrift Für Kristallographie New Crystal Structures, 238(5), 911–913. https://doi.org/10.1515/ncrs-2023-0270
- 29 Fatmah A. M. Al-Omary, Alanazi, F. S., Ghabbour, H. A., & El-Emam, A. A. (2016). Crystal structure of 2-[3,5-bis(trifluoromethyl)benzylsulfanyl]-5-(5bromothiophen-2-yl)-1,3,4-oxadiazole,

- C15H7BrF6N2OS2. Zeitschrift Für Kristallographie New Crystal Structures, 232(1), 131–133. https://doi.org/10.1515/ncrs-2016-0188
- 30. Kupka, T., Buczek, A., Broda, M. A., Michał Stachów, & Tarnowski, P. (2016). DFT studies on the structural and vibrational properties of polyenes. Journal of Molecular Modeling, 22(5), 101-111. https://doi.org/10.1007/s00894-016-2969-1
- 31 Silverstein, Robert M., Bassler, G., Clayton Webster, Francis X., Morrill., & Terence C, (2022) Spectrometric identification of organic compounds, New Delhi, Wiley India
- 32 Fatmah A. M. Al-Omary, Olivier Blacque, Alanazi, F. S., Edward, & El-Emam, A. A. (2023). Crystal structure of 2-[(4-bromobenzyl)thio]-5-(5-bromothiophen-2-yl)-1,3,4-oxadiazole, C13H8Br2N2OS2. Zeitschrift Für Kristallographie New Crystal Structures, 238(5), 911–913. https://doi.org/10.1515/ncrs-2023-0270
- Siluvairaj, R. R., Vallal Perumal Govindasamy, Rajarajan Govindasamy, Periyanayagasamy Vanathu Chinnappan, & Venugopal, T. (2024). Comparative study of 4-((4-aminophenyl)diazenyl)-2-((2phenylhydrazono)methyl)phenol and N-(4-((4-hydroxy-3-((2
  - phenylhydrazono)methyl)phenyl)diazenyl)phenyl)acetami de-DFT method. European Journal of Chemistry, 15(1), 50–70. https://doi.org/10.5155/eurjchem.15.1.50-70.2498
- 34. Ali, A., Khalid, M., Tahir, M. N., Imran, M., Ashfaq, M., Hussain, R., Assiri, M. A., & Khan, I. (2021). Synthesis of Diaminopyrimidine Sulfonate Derivatives and Exploration of Their Structural and Quantum Chemical Insights via SC-XRD and the DFT Approach. ACS Omega, 6(10), 7047–7057. https://doi.org/10.1021/acsomega.0c06323
- 35 Hasan Tanak. (2011). DFT computational modeling studies on 4-(2,3-Dihydroxybenzylideneamino)-3-methyl-1H-1,2,4-triazol-5(4H)-one. Computational and Theoretical Chemistry, 967(1), 93–101. https://doi.org/10.1016/j.comptc.2011.03.048
- 36. Özdemir, M., Sönmez, M., Şen, F., Dinçer, M., & Özdemir, N. (2015). A novel one-pot synthesis of heterocyclic compound (4-benzoyl-5-phenyl-2-(pyridin-2-yl)-3,3a-dihydropyrazolo[1,5-c]pyrimidin-7(6H)-one): Structural (X-ray and DFT) and spectroscopic (FT-IR, NMR, UV-Vis and Mass) characterization Studies. Spectrochimica Acta Part A: Molecular and Biomolecular Spectroscopy, 137, 1304–1314. https://doi.org/10.1016/j.saa.2014.08.131
- 37 Al-Abdullah, E. S., Mary, Y. S., Panicker, C. Y., El-Brollosy, N. R., El-Emam, A. A., Alsenoy, C. V., & Al-Saadi, A. A. (2014). Theoretical investigations on the molecular structure, vibrational spectra, HOMO–LUMO analyses and NBO study of 1-[(Cyclopropylmethoxy)methyl]-5-ethyl-6-(4-methylbenzyl)-1,2,3,4-tetrahydropyrimidine-2,4-dione. Spectroscimica Acta Part a Molecular and Biomolecular Spectroscopy, 133, 639–650. https://doi.org/10.1016/j.saa.2014.06.042
- 38 Raczyńska, E. D., Hallman, M., Katarzyna Kolczyńska, & Stępniewski, T. M. (2010). On the Harmonic Oscillator Model of Electron Delocalization (HOMED) Index and its Application to Heteroatomic π-Electron Systems. Symmetry, 2(3), 1485–1509. https://doi.org/10.3390/sym2031485
- 39 Kolandaivel, P., Praveena, G., & Selvarengan, P. (2005). Study of atomic and condensed atomic indices for reactive sites of molecules. Journal of Chemical Sciences, 117(5), 591–598. https://doi.org/10.1007/bf02708366
- 40. Okulik, N., & Jubert, A. H (2005). Theoretical analysis of the reactive sites of non- steroidal antiinflammatory drugs, Internet Electronic Journal of Molecular Design., 4, 17–30
- 41. Ajibade Ādejoro, I., Emmanuel Oyeneyin, O., & Temitope Ogunyemi, B. (2015). Computational

Investigation on Substituent and Solvent Effects on the Electronic, Geometric and Spectroscopic Properties of Azobenzene and Some Substituted Derivatives. International Journal of Computational and Theoretical Chemistry, 3(6), 50. https://doi.org/10.11648/j.ijctc.20150306.12

- 42. Politzer, P., Concha, M. C., & Murray, J. S. (2000). Density functional study of dimers of dimethylnitramine. International Journal of Quantum Chemistry, 80(2), 184–192. https://doi.org/10.1002/1097-461x(2000)80:2%3C184::aid-qua12%3E3.0.co;2-o
- Feixas, F.; Matito, E.; Poater, J.; Solà, M. Quantifying aromaticity with electron delocalisation measures. Chem. Soc. Rev. 2015, 44, 6434 6451.
- Stanger, A. Nucleus-independent chemical shifts (NICS):
  Distance dependence and revised criteria for aromaticity and antiaromaticity. J. Org. Chem. 2006, 71, 883–893.